Accepted Manuscript

Twenty-first Century central Rocky Mountain River discharge scenarios under greenhouse forcing

Jeannine-Marie St. Jacques, Suzan L. Lapp, Yang Zhao, Elaine M. Barrow, David J. Sauchyn

PII: S1040-6182(12)00443-0

DOI: 10.1016/j.quaint.2012.06.023

Reference: JQI 3389

To appear in: *Quaternary International*

Received Date: 13 July 2011

Revised Date: 22 May 2012

Accepted Date: 18 June 2012

Please cite this article as: St. Jacques, J.-M., Lapp, S.L., Zhao, Y., Barrow, E.M., Sauchyn, D.J., Twenty-first Century central Rocky Mountain River discharge scenarios under greenhouse forcing, *Quaternary International* (2012), doi: 10.1016/j.quaint.2012.06.023.

This is a PDF file of an unedited manuscript that has been accepted for publication. As a service to our customers we are providing this early version of the manuscript. The manuscript will undergo copyediting, typesetting, and review of the resulting proof before it is published in its final form. Please note that during the production process errors may be discovered which could affect the content, and all legal disclaimers that apply to the journal pertain.

ACCEPTED MANUSCRIPT

Twenty-first Century Central Rocky Mountain River Discharge Scenarios under Greenhouse Forcing

Jeannine-Marie St. Jacques[1*], *Suzan L. Lapp*[1], *Yang Zhao*[2],

Elaine M. Barrow[1], *David J. Sauchyn*[1]

[1] Prairie Adaptation Research Collaborative (P.A.R.C.), Room 120, 2 Research Drive, University of Regina, Regina, Saskatchewan, Canada, S4S 7H9

[2] Department of Mathematics and Statistics, University of Regina, Regina, Saskatchewan, Canada, S4S 0A2

*Corresponding author: stjacqje@uregina.ca

Abstract

The present-day hydroclimatology of the central Rocky Mountains is heavily influenced by recurring large-scale climate patterns: the Pacific Decadal Oscillation (PDO), the El Niño-Southern Oscillation (ENSO), and the Arctic Oscillation/North Atlantic Oscillation (AO/NAO). Hence, low frequency central Rocky Mountain river discharge variability can be successfully modeled by regression techniques using these climate indices as predictors. Generalized Least Squares (GLS) regression equations captured a large portion of streamflow variability at the hydrological apex of North America. Using archived runs from global climate models from the IPCC Fourth Assessment Report (AR4) (Phase 3 of the Coupled Model Intercomparison Project - CMIP3), the PDO, ENSO and the NAO were projected for the 21st century for the B1, A1B and A2 Special Report on Emission Scenarios (SRES). These projected climate indices were used as inputs into the GLS regression equations, giving projected central Rocky Mountains river discharges. These projections showed generally declining trends in central Rocky Mountains surface water availability for 2006-2050 and 2006-2096. This study's novel result is that projection distribution functions show a shift in the variance of the flows, from a relatively symmetric equal probability of low versus high flows about the mode and mean in 2006, to a broader, left-skewed flow pattern with a higher probability of low flows in general, and extreme low flows in particular, by 2096.

Keywords: *El Niño-Southern Oscillation (ENSO), Generalized Least Squares (GLS) regression models, North Atlantic Oscillation (NAO), Pacific Decadal Oscillation (PDO), projected river discharge, central Rocky Mountains.*

1 Introduction

Central Rocky Mountain hydroclimatology is heavily influenced by recurring large-scale climate patterns: the Pacific Decadal Oscillation (PDO), the El Niño-Southern Oscillation

ACCEPTED MANUSCRIPT

(ENSO), and the Arctic Oscillation (AO). Strong periodic cycles are associated with the low-frequency PDO in much of the western North American hydroclimate (Mantua et al., 1997; Stewart et al., 2005; St. Jacques et al., 2010). The PDO is an integrated measure of North Pacific oceanic and atmospheric variability that shifts phases on an inter-decadal time scale, usually ~30 years (Minobe, 1997; Mantua and Hare, 2002). In the central Rocky Mountains, a strong negative relationship exists between the PDO and winter precipitation, and subsequently between the PDO and streamflow (Mantua et al., 1997; Comeau et al., 2009; Wise, 2010). The higher frequency ENSO also affects the hydroclimatology of this region as precipitation and streamflow are decreased during El Niño events and increased during La Niña events (Shabbar and Khandekar, 1996; Shabbar et al., 1997; Bonsal and Lawford, 1999; Bonsal et al., 2001; Shabbar and Skinner, 2004; Bonsal and Shabbar, 2008). The AO is a measure of the intensity of the polar vortex and is closely related to (if not the same as) the North Atlantic Oscillation (NAO) (Wallace and Gutzler, 1981). A negative relationship exists between Canadian Prairie Provinces' winter precipitation and the NAO (and AO), as more frequent outbreaks of cold, dry Arctic air occur with the positive NAO (and AO) (Bonsal and Shabbar, 2008).

Under anthropogenic global warming scenarios, decreased streamflow is projected in the central Rocky Mountains (see Fig. 10.12, IPCC4, 2007, for multi-model mean run-off changes). St. Jacques et al. (2010) analyzed southern Alberta, and adjacent British Columbia and Montana, streamflow records for any significant existing trends attributable to global warming, while explicitly including the possible effects of the PDO and interannual regional circulation anomalies (i.e., ENSO, NAO) to account for naturally-occurring hydroclimatic variability. They concluded that streamflows are declining at most gauges due to hydroclimatic changes (probably from global warming) and, in some cases, intensive use of surface water resources, which were of the same order of magnitude as the changes in the hydrologic regime, if not greater. In the process, they developed Generalized Least Squares (GLS) regression models which explained a large amount of the variance in regional river discharge as a function of the PDO, ENSO and the NAO. This paper takes their best-fitting river discharge models, adds more models from additional gauges and uses these empirical models to project central Rocky Mountain river discharges for the 21st century. Lapp et al. (2012) developed 21st century projections of the PDO, ENSO and NAO from archived runs of global climate models (GCMs) from the IPCC Fourth Assessment Report (AR4) (Phase 3 of the Coupled Model Intercomparison Project - CMIP3). These climate oscillation projections were used as inputs into the GLS regression equations to produce projected central Rocky Mountain river discharges for 2006-2096. These projections should be regarded as scenarios or as a thought-experiment, since these extrapolations assume no change in the regional physical hydrology and water management practices, but are useful explorations of the consequences of global warming, including the future status of teleconnections, and of current trends and water management practices.

2 Methods

2.1 *River discharge modeling and projection*

Six actual (recorded) stream discharge records and three naturalized discharge records in the central Rocky Mountains analyzed by St. Jacques et al. (2010), together with two additional

ACCEPTED MANUSCRIPT

actual stream discharge records from the same region, were chosen based on the large amount of variance of observed 20th century discharge (i.e., high R^2) explained by the GLS models (Figure 1, Tables 1 and 2). Four of the gauges, those on the Waterton, Elk, Marias and North Fork of the Flathead Rivers, are on unregulated or slightly regulated reaches. Three of the gauges measure regulated flows on the Oldman, St. Mary and Belly Rivers, and in these cases, both the observed actual flows and the reconstructed naturalized flows were separately analyzed, providing an additional six records. For one regulated gauge, on the South Saskatchewan River, only the recorded flow was analyzed, as the naturalized record did not have as good a fit to the GLS model. Five of the gauges are located in southern Alberta, one in southern British Columbia, and two in adjacent Montana. All records span at least 73 years. The gauges are located at the hydrographic apex of North America, with headwater streams flowing to the Arctic, Atlantic, and Pacific Oceans (Rood et al., 2005). The Waterton, St. Mary and Belly Rivers are tributaries of the Oldman River, which in turn, is a tributary of the South Saskatchewan, the major regional river.

Streamflow records were extracted from the databases of the Water Survey of Canada (HYDAT; http://www.wsc.ec.gc.ca/applications/H2O/index-eng.cfm, July 12, 2011) and the U.S. National Water Information System (http://waterdata.usgs.gov/nwis/sw, July 12, 2011). In addition to gauge records from unregulated streams, a streamflow database produced by Alberta Environment provided naturalized daily flows and void-filled records to overcome the effects of human impacts and gaps in the time series, respectively (Alberta Environmental Protection, 1998). Mean daily flows averaged over the year were used.

Following St. Jacques et al. (2010), the models included as predictors a linear trend and three climate indices: the PDO, ENSO, and the NAO, as a proxy for the AO record. The winter averaged (November-March) PDO was computed from the HadSST2 dataset of sea surface temperatures (SST) (Rayner et al., 2003) following the method outlined in Lapp et al. (2012). The annually averaged Southern Oscillation Index (SOI) (used as an ENSO metric) and the winter averaged (December-March) NAO were obtained from the Earth Systems Research Laboratory (National Oceanic and Atmospheric Administration, www.cdc.noaa.gov/ClimateIndices/, July 12, 2011). Since streamflow is naturally lagged and smoothed from precipitation by surface and subsurface hydrology, and large-scale climatic phenomena act most prominently at inter-annual time scales, the stream observations were lagged relative to the climate indices by 0, ±1, and +2 years, and a binomial smoother of five years was applied to both the stream and climate data. The climate indices and their lags showed only minor collinearity.

Generalized Least Squares (GLS) computes time series regression with serially correlated residuals and is therefore suitable for hydrological data (Brockwell and Davis, 2002). Autoregressive-moving-average (ARMA(p,q)) models were fit to the residuals using a Maximum Likelihood Estimator. Open-source software from the R statistical programming language (version 2.9.1) was used, specifically the *arima* function in the {*stats*} package (R Development Core Team, 2008).

The statistical model used in this study is

$$Q_t = \mu + \lambda T_t + \beta_1 x_{1,t} + \ldots + \beta_k x_{k,t} + \varepsilon_t, \qquad t = 1,\ldots, L,$$

ACCEPTED MANUSCRIPT

where $\{Q_t\}$ is mean daily streamflow for year t, index t runs over L years; μ is the mean streamflow over all L of these years; T_t is a linear trend with coefficient λ representing the trend to be detected; $\{x_{i,t},\ t = 1,\ldots,L\}$ is the i^{th} explanatory variable; k is the number of explanatory variables; β_i is the coefficient for the i^{th} explanatory variable; and $\{\varepsilon_t\}$ is the residual time series, which is an autoregressive-moving average process of order (p,q) (ARMA(p,q)). An optimum minimal subset of significant predictors and an optimum minimal ARMA(p,q) residual model was chosen using the corrected Akaike Information Criterion (AIC_c) goodness-of-fit statistic (Brockwell and Davis, 2002) applied to all predictor subsets of size ≤ 6, and for all $p \leq 8$ and $q \leq 5$. When the optimum minimal ARMA(p,q) residual model had $p + q > 5$, the model was examined for overfitting using the methods described in *sec. 8.2* of Cryer and Chan (2008) and adjusted accordingly to the ARMA(p,q) residual model with the next smallest AIC_c, if appropriate. Because in GLS regression an ARMA(p,q) model is fit to the residual error, an estimate of the error can be projected into the future and added to the extrapolated future value derived from the regression equation alone, improving the projection (Cryer and Chan, 2008). Residual errors were projected for all regression models, until the projected errors' absolute value were less than 0.05. The non-zero significance of the trend coefficient λ was tested by the Neyman-Pearson statistic (RP) (Zheng et al., 1997) using the null model of the optimum set of explanatory variables (minus the trend variable if included in the optimum set) versus the alternative model of the optimum set of explanatory variables together with the linear trend (if not already added). The RP is asymptotically distributed as a chi-square distribution with one degree of freedom. If the estimated RP is greater than the 0.10 percentile of $\chi^2_{(1)}$, the trend is significant at the 90% level. Shapiro-Wilk tests on the innovations confirmed that most were normally distributed, and that departures from normality were mild.

2.2 *How the climate indices were calculated and projected*

2.2.1 Choice of GCMs

International modeling centers have submitted their projections for the 21st century under different emissions scenarios, simulations of 20th century climate and pre-industrial control runs to scrutiny by the wider scientific community (Meehl et al., 2007). These data from 23 GCMs are archived by the Program for Climate Model Diagnosis and Intercomparison (PCMDI) of Lawrence Livermore National Laboratory (http://www-pcmdi.llnl.gov/ipcc/about_ipcc.php, July 12, 2011). Details of the GCMs are found in IPCC4 (2007), Table 8.1. Because of the importance of recurring large-scale climate patterns (i.e., the PDO, ENSO, NAO) on surface climate, these CMIP3 runs have been critically examined for their ability to model these atmosphere-ocean climate oscillations. Lapp et al. (2012) and Furtado et al. (2011) were the first to explicitly project the PDO, as calculated by EOF analysis of North Pacific SST residuals, as defined by Mantua et al. (1997) and Zhang et al. (1997). From the 23 GCMs with archived data, Lapp et al. (2012) chose the 10 models best able to simulate the PDO, ENSO, and NAO, using comparisons among the 20th century observed records and the 20th century simulation runs (Table 3). They selected model runs under the low B1, moderate A1B and high A2 emissions scenarios (Nakicenovic et al., 2000).

2.2.2 Calculation of the PDO for 1900-2099 from observed and GCM data

ACCEPTED MANUSCRIPT

For the calculation of the PDO from the observed instrumental data, Lapp et al. (2012) followed the method described in Mantua et al. (1997), Zhang et al. (1997), and Mantua and Hare (2002). Their PDO index was the leading Principal Component (PC) time series from an un-rotated EOF analysis of monthly, "residual" North Pacific SST anomalies, poleward of 20^{o} N for the 1900-1993 time period. "Residuals" are the difference between the observed SST anomalies and the monthly mean global average SST anomaly (Zhang et al., 1997). The PDO index for 1994-2008 was calculated by projecting the 1994-2008 residual SST anomalies onto the leading eigenvector or loading pattern (EOF 1) from the 1900-1993 SST data. Likewise, the projected PDO indices for 2000-2099 were calculated by projecting the 2000-2099 residual SST anomalies from each of the GCMs onto the leading eigenvector (EOF 1) from the 1900-1993 GCM SST data.

The 21st century winter PDO projections showed a shift towards more occurrences of the negative phase PDO, non-significant for 2000-2050, but significant for 2000-2099, for all three emissions scenarios (Table 4) (Lapp et al., 2012). This can be seen by comparing the all-model 1900-1999 simulation mean to the 2000-2050 and 2000-2099 all-model means (Table 4). Under the more severe A2 emissions scenario, the shift towards more negative phase PDO occurrences was most pronounced. Comparison of the all-model 1900-1999 simulation means to the actual 1900-1999 observed mean PDO index showed that that the GCMs have a slight bias towards the negative PDO phase (Table 4).

2.2.3 Calculation and projections of the SOI and NAO

The annual SOI was calculated as the difference between monthly mean sea level pressure (SLP) at Tahiti, Polynesia (17.5^{o} S, 149.6^{o} W), and Darwin, Australia (12.4^{o} N, 130.9^{o} E), with the difference normalized relative to 1951-1980 (Ropelewski and Jones, 1987). The early 21st century (2000-2050) SOI projections showed a shift towards a climate with more occurrences of El Niño (negative SOI) and decreases in the occurrences of La Niña (positive SOI) for all emissions scenarios, significantly for the B1 scenario (Table 4) (Lapp et al., 2012). However, the entire 21st century (2000-2099) SOI projections showed a significant shift towards a climate with more occurrences of El Niño for the B1 emissions scenario, but shifts towards more occurrences of La Niña for the A1B and A2 scenarios, non-significantly for the former, and significantly for the latter (Table 4). Likewise, the winter NAO index was calculated as the difference between monthly mean SLP at Gibraltar, Spain (36.1^{o} N, 5.2^{o} W), and Reykjavik, Iceland (64.1^{o} N, 21.6^{o} W), each normalized relative to 1951-1980 before differencing (Jones et al., 1997). The 21st century NAO projections showed a shift towards a climate with more occurrences of the positive phase of the NAO (positive AO) and decreases in the occurrences of the negative NAO (negative AO) for all three emissions scenarios, a shift significant at the $p \leq 0.05$ level for the A1B and A2 scenarios for both 2000-2050 and 2000-2099 (Table 4) (Lapp et al., 2012).

2.2.4 Streamflow projection assessment methods

In order to determine if significant changes in streamflow were projected for each emissions scenario, GLS trend lines were fit using the R Programming Language to the all-model mean streamflows for the 11 mean daily discharge records for two time periods: 2006-2050 and 2006-2096, and the significance of the trend term coefficient β_1 was assessed using the

ACCEPTED MANUSCRIPT

coefficient variance-covariance matrix (i.e., whether or not the interval (β_1 ± 1.96* standard deviation) contains zero). Extrapolations to mid-century are not unreasonable, given the shortness of the intervening interval; extrapolations to century's end are more speculative, but still worth exploring. A commencement year of 2006 was used because the GLS regressions have the common form of a linear regression equation together with projected ARMA error term in this time period (prior to 2006 there can be no ARMA error term as the GCMs do not explicitly include modeled rivers). Discharge projections end at 2096 (not 2099) due to the use of five-year binomially smoothed predictors with leads and lags. In order to compare changes across records, the magnitude of the changes in estimated mean daily flows over the projection periods of 2006-2050 and 2006-2096 were calculated as percentage changes *per annum*: $\Delta/yr = 100*\beta_1/mean(Q)$, where *mean(Q)* is computed over the appropriate 21st century time period (Rood et al., 2005).

Ensembles of climate projections are frequently used to describe prediction uncertainties arising from different GCM constructions, differing initial conditions, and unknown future greenhouse emissions. In this study, each of the 11 river discharge records is forecast by an ensemble consisting of a total of 51 GCM streamflow projections drawn from ten GCMs, several of which have multiple runs from different initial conditions, and three emissions scenarios. A typical climate-change ensemble produces a collection of irregular, often tangled, time series or "spaghetti" (Dettinger, 2005). In order to focus on the most likely changes, rather than just the possible or extreme changes, a balanced, quantitative assessment of the spaghetti of an ensemble requires an estimation of the underlying projection distribution function (PDF), as the best available approximation of the actual climate-change probability distribution function (Dettinger, 2005; 2006). Smoothed PDFs were estimated by the resampling approach of Dettinger (2005; 2006) based upon principal components analysis (PCA), which generates a large number of additional time series or realizations which share important first- and second-order statistical characteristics with the original ensemble. For each river discharge record, the PCA components were resampled 20,000 times, generating an additional climate-change "projection" realization each time. Following Dettinger (2005, 2006), mixing of the ensemble loading patterns was restricted to only allow intermixing of projections by a single GCM at a time. The realizations were ranked and summarized in histograms to obtain PDFs for 2006, 2050 and 2096. In order to provide flow probabilities for risk analysis and water management, empirical cumulative distribution functions (CDFs) were constructed from the PDFs (Wilks, 2006). All of these calculations were done with MATLAB® Release 2011a.

3 Results

3.1 *GLS river discharge modeling from observed 20th century data*

The GLS regression analysis of the observed streamflow data showed a regional pattern of declining flows in the 20th century (Tables 1 and 2, and Figure 2). Eight of the 11 regression models revealed significant declining trends, with the exceptions being the North Fork of the Flathead, the naturalized St. Mary and the naturalized Belly discharge records, which showed no significant trends at the 10% level in the 20th century. Three of the gauge records in relatively undisturbed watersheds, the Elk, Marias and Waterton Rivers, showed significant declines, as did the naturalized Oldman River, which indicates that the declines are not purely due to direct human impact, but also to hydroclimatic causes, presumably global warming. The current year

ACCEPTED MANUSCRIPT

PDO or a lead or lag was the explanatory variable that always appeared in the optimum predictor set (Table 2). Because the predictor variables were standardized to zero mean and unit standard deviation, the relative importance of the predictors can be assessed by comparing the regression coefficients. This showed that the declining trend and the PDO were the most influential predictors. The majority of the 20th century low frequency variance (i.e., that passed by a five-year binomial smoother) was captured by the GLS regression models. The mean R^2_{regular} was 0.56, with R^2_{regular} computed as 1 – (sum-of-squares of simple regression residuals/total-sum-of-squares), i.e., without modeled error adjustment (Table 2). Also shown in Table 2 are the large improvements in the coefficient of determination, $R^2_{\text{innovations}}$, that result from ARMA modeling of the error during the period of record. When $R^2_{\text{innovations}}$ was computed with the modeled error adjustment, as 1 – (sum-of-squares of innovations/total-sum-of-squares), its mean was 0.71. In this study, a large number of the longest, naturally-flowing Pacific Northwest and Rocky Mountain rivers were examined for their suitability for similar GLS regression models (Slack and Landwehr, 1992; Harvey et al., 1999; Rood et al., 2005). Most had very high $R^2_{\text{innovations}}$, but much lower R^2_{regular}; therefore, they were not used for 21st century projections as the ARMA error term can be only projected ~30 years before it decays. Plots of the 11 discharge records, together with the fitted regression models, show that the low frequency variance was captured well, with the extreme flows being captured less well (Figure 2). ARMA(p, q) models where $p \geq 2$ and $q \geq 1$ most frequently fitted the error terms, showing the importance of multi-year persistence. All records had no near-unit autoregressive roots, which suggested that ARMA residuals are appropriate.

This study found a greater prevalence of declining significant trends than the earlier study of St. Jacques et al. (2010) using many of the same discharge records (Table 1). This is attributed to the use of the later compiled and more complete HadSST2 dataset in the construction of the PDO index, which more accurately represents the historic North Pacific pattern of variability. St. Jacques et al. (2010) used Mantua's PDO index in their analysis which is based upon the earlier and less complete HadSST1 dataset (Mantua et al., 1997).

3.2 *Central Rocky Mountain projected streamflows to mid- and late-21st century*

Our GLS regression modeling approach based upon GCM projected climate indices indicated generally declining trends in projected central Rocky Mountain surface water availability for both the first half of the 21st century and over its entirety (Table 5 and Figure 3 which presents the results for the A1B scenarios, the others are not shown as they are similar). Six of the 11 models, those of the Elk, Marias, St. Mary, Oldman, naturalized Oldman and South Saskatchewan gauge records, showed declining trends in the all-model mean projections regardless of the time period considered for all three emissions scenarios at the 95% significance level. This is summarized in Figure 4 which shows representative rivers from each of the three drainages, and their simulations and projections for each of the three emission scenarios. The other five models showed primarily no significant trends or decreases, with four increases, all over the longer 2006-2096 time period (Table 5). As first observed in the instrumental records, three of the four gauge records in relatively undisturbed watersheds, the Elk, Marias and Waterton Rivers, showed continued projected declines (as did the naturalized Oldman River) which suggests that the declines are not purely due to continued direct human impact, but also to global warming. As well, these three projections of actual discharge records with little direct

ACCEPTED MANUSCRIPT

human impact showed relatively low decline rates compared to those of some of the regulated flows (Table 5). At the regulated gauges, the all-model mean projections based upon the actual flows showed much steeper declines than the all-model mean projections based upon the naturalized flows (when included in the analysis). The all-model mean projection based upon the actual flow record for the Oldman River at Lethbridge showed the steepest rate of decline, approaching zero flow at the end of the 21st century (figure not shown). Streamflow trends were broadly similar across all three emissions scenarios, but the A2 emissions scenario showed the most significant increasing trends among the three when considered for the entire century (Table 5).

Time slices of the PDFs of a 20,000-member resampling of the 51-member projection ensemble are shown for 2006, 2050 and 2096 for each of the 11 central Rocky Mountain river records (Figure 5). The PDFs for all of the discharge records, except for the naturalized Belly River, shift from relatively symmetric distributions in 2006 towards broader, left-skewed distributions with modal peaks centered at lower discharges by 2096. This left-skewness suggests that extreme low flows will become more frequent. Since five-year binomially smoothed data are analyzed, these are conservative estimates. The increasing spread over the entire 21st century seen in all 11 PDFs is a result of increasing variance in the projected PDO, SOI and NAO indices (i.e., the input variables in the GLS models), and increasing divergence among the GCMs and the emissions scenarios. The PDF for the naturalized Belly record shows a shift towards a modal peak centered at a higher discharge by 2050, a tendency that continues through 2096.

In a corresponding fashion, the empirical CDFs for eight of the discharge records, the Elk, Marias, St. Mary, Belly, Waterton, Oldman, naturalized Oldman and South Saskatchewan Rivers, shift to the left from 2006 to 2050, and continue to move leftwards through to 2096, with the Oldman River showing a noticeable non-zero probability of negative discharges by 2050, and the Marias, St. Mary, Oldman and South Saskatchewan Rivers showing negative (i.e., zero) flow by 2096 (partially shown in Figure 6). These negative flows are interpreted as demonstrating a significant probability of a dry watercourse, assuming 20th century hydrology and water management practices. For the Oldman River, this probability is 5% by 2050, which grows to 38% by 2096; for the South Saskatchewan, this probability is 1% by 2050, which grows to 10% by 2096; for the St. Mary River, it is 6% by 2096; and for the Marias River, it is 2% by 2096. The Flathead and naturalized St. Mary CDFs show leftward shifts from 2006 to 2050, and then shift rightward back to their 2006 position by 2096, except for slightly more variance in 2096; whereas the naturalized Belly CDF shows definite right shifts from 2006 to 2050 and then again from 2050 to 2096 (results not shown).

4 Discussion

This study suggests a declining availability of surface water supplies for the central Rocky Mountains for the 21st century based on river discharges projected using GLS regression models with GCM-derived climate oscillations as predictor variables (Table 2). This study also suggests that any deleterious effects of global warming on surface water supplies are only compounded by the drawdown effects of direct human impacts, which are of at least a similar order of magnitude, as shown by comparison of trends in paired actual and naturalized flow records (Figure 3, Table 5). This declining availability is particularly illustrated by the projection

of the actual flow of the South Saskatchewan River, the major regional river and an acknowledged over-allocated system (Rood and Vandersteen, 2010), which has a 1% probability of zero flows by 2050, which becomes 10% by the end of the 21st century (Figures 3, 5 and 6). Time slices of the projection distribution functions (PDFs), the best available approximation of the actual climate-change probability distribution functions, also show a change in the variance of the smoothed flows, from a relatively symmetric equal probability of low versus high flows about the mode and mean in 2006, to a broader, more variable flow pattern with a higher probability of flows less than the mode by 2050, a tendency which generally continues and increases by 2096 (Figure 5).

For the climatological context of these hydrological projections, Barrow (2010) examined Second Coupled Model Intercomparison Project (CMIP2) GCM projections for temperature and precipitation for southern Alberta and Saskatchewan. These projections showed median increases in annual mean temperature of 4^{o} to 6^{o} C by 2070-2099, with maximum annual mean temperature increases of between 6^{o} and 8^{o} C. Minimum annual precipitation changes indicate slight decreases of 0-10% across the southern Prairies throughout the 21st century; however, median and maximum changes suggest annual increases in regional precipitation. There is a projected seasonal shift in precipitation from summer to winter (Barrow, 2010).

Climate model projections due to anthropogenic climate change in this century are uncertain because of model differences in parameterization and initialization, unknown future greenhouse gas emissions and the chaotic nature of the global climate system. Dettinger (2005; 2006) has proposed that the focus of regional climate prediction should change from a concentration on what is possible to that which is more likely. He promotes using a multiple-model, multiple-emissions ensemble of the most recent available climate change scenarios to characterize the overall distributions of the climate-change projections or PDFs, rather than focusing on the results from a few or extreme projections. It is his approach that this study follows to obtain our novel result of a change in the projected flow variance, from a relatively symmetric equal probability of low versus high flows about the mode and mean in 2006, to a broader, more variable flow pattern with a higher probability of flows less than the mode by 2096 (Figure 5).

This study's result of projected declining flows are compatible with the extrapolation of declining trends in the observed centennial-length instrumental records (e.g., Zhang et al., 2001; Rood et al., 2005; 2008; Schindler and Donahue, 2006; St. Jacques et al., 2010; Shepherd et al., 2010). For comparison, the instrumental climate records from 1900-1998 show that the headwater region has experienced increased daily maximum and minimum temperatures and increased annual precipitation (Zhang et al., 2000). This present study is also in accord with Schindler and Donahue (2006) and St. Jacques et al. (2010) that any deleterious effects of global warming on regional surface water supplies are only compounded by the drawdown effects of direct human impacts.

Low-frequency variability (i.e., slightly smoothed data) was analyzed because of the associated severe socio-economic and ecological impacts of prolonged drought. Conventional risk mitigation strategies (insurance, reservoir storage, etc.) can accommodate high-frequency variability in precipitation and streamflow, but not low-frequency variability (i.e., sustained drought), which is a much more challenging climate hazard. The region has reservoir capacity

for a drought of a year or two, but not longer (*pers. comm.* Michael Senaka, Alberta Environment).

This study used GCM-derived atmosphere-ocean climate indices as predictors in statistical hydrological models (Vicuna and Dracup, 2007). Our statistical model captures the hydroclimatic variability over the entire centennial-length instrumental record which allows inclusion of the effects of low frequency climate variability such as that of the PDO. This regression-based projection approach is not without precedent: Stewart et al. (2004) developed a similar ordinary least squares regression-based projection of changes in western North American snowmelt runoff timing, using downscaled GCM-projected temperature and precipitation data as predictors. Regression-based approaches using atmosphere-ocean climate oscillations, such as ENSO, or other oceanic variables, have been used in many regions of the globe to successfully forecast short-term streamflow (e.g., Ruiz et al., 2007; Xu et al., 2007; Lima and Lall, 2010). Because regression models are relatively fast and easy to build, it is feasible to construct many such models, enabling coverage of a wide geographical area. A limitation of these statistical approaches is that they do not explicitly account for the physical mechanisms and processes that define basin-scale hydrological response to climate forcing. The use of GCM temperature and precipitation projections (with or without downscaling) as predictors in physically-based hydrologic models (e.g., Dettinger et al., 2004; Lapp et al., 2009; Shepherd et al., 2010; Larson et al., 2011; Kienzle et al., 2012) is typically labor- and time-intensive, requiring detailed basin physical characteristics and climate data for model parameterization, calibration and validation. The central Rocky Mountain rivers are largely fed by snowmelt at high elevations. Snowpack accumulation and climate monitoring data are sparse, if they even exist, and are certainly not available at a density to adequately represent spatially this very climatologically heterogeneous region. These data constraints generally limit the calibration data to the period of satellite remote sensing datasets for estimating snowcover, land-use, vegetation extent and type, etc. (Day, 2009). Therefore the full extent of instrumental climatological and hydrological variability, as brief and unrepresentative it is (as shown by proxy-based paleoclimatic records, e.g., Axelson et al., 2010; Sauchyn et al., 2011), is not applied to the physically-based hydrologic models. Thus, the statistical hydrological models and the physically-based watershed models form two complimentary approaches, each with its own advantages and limitations. If the two approaches converge on a common projected result, this lends confidence to both.

This study's results are broadly consistent with other related work on regional trends in projected streamflow using physically-based hydrologic models (i.e., Lapp et al., 2009; Shepherd et al., 2010; Larson et al., 2011; Tanzeeba and Gan, 2012). Lapp et al. (2009) generated scenarios of future flows of the South Saskatchewan River at Lake Diefenbaker and its tributaries, the Bow, Red Deer and Oldman Rivers, under the SRES A2 emissions scenario by coupling the HadCM3 GCM with the hydrological WATFLOOD model. When comparing 2040-2069 mean projected data to 1961-1990 baseline data, Lapp et al. (2009) found projected annual flow decreases in all rivers (an average decline of -7%), and a shift in the dominant flow to earlier in the year in all rivers. Similarly, Shepherd et al. (2010) drove the physical models MTCLIM, SNOPAC and RIVRQ with statistically-downscaled global circulation data from six recent CMIP2 and CMIP3 GCMs to project Rocky Mountain rivers, including the Belly, Waterton, naturalized Oldman, and naturalized St. Mary Rivers, for the first half of the 21st century under the SRES A2 emissions scenario. They found that summer flows are projected to

decline considerably, while winter and early spring flows are projected to increase, with an overall decline in annual discharge of -3% over 2005-2055. On the other hand, Larson et al. (2012) and MacDonald et al. (2011) projected decreases in spring flows from snowmelt for the 21st century, using delta-method downscaled GCM data over a range of SRES emissions scenarios as inputs into the hydrological models SIMGRID to model spring runoff from snowpack, and GENESYS to model snowpack, respectively, in the fully allocated St. Mary River watershed of Montana and Alberta. The delta-method applies monthly changes from GCM data to observed climate data (typically from 1961-1990) and does not therefore include projected changes in climate variability (MacDonald et al., 2011). Since mountain snowpack provides so much of the total annual discharge in these mountain rivers, the declining spring meltwater volumes projected in these studies would be consistent with our study's projected declines in annual discharge. Tanzeeba and Gan (2012) projected decreases in future annual and summer streamflow and snow water equivalent, and an earlier onset of spring runoff, despite projected precipitation increases in the South Saskatchewan River Basin. They found that the projected increase in evaporation loss due to a warmer climate will offset the precipitation increases. They used a land surface scheme driven by delta-method downscaled GCM data over a range of SRES emissions scenarios as inputs into the hydrological model. Overall, a diverse suite of hydrological modeling methods are all projecting declining surface water availability in the 21st century for the region. However, only our study explicitly models the interannual to decadal-scale hydroclimate variability and the influence of large-scale climate oscillations (teleconnections) on Rocky Mountain surface hydrology. Thus the study is able to project both trends in mean runoff and shifts in the frequency of extreme annual flows.

In our results, the declining trend and PDO terms were the most influential predictors among those examined (Table 2). All of the PDO terms had negative coefficients in the GLS regression models (Table 2) and therefore modeled increasing discharge when the PDO index is negative and decreasing discharge when the PDO index is positive. Lapp et al. (2012) showed a statistically significant multi-model mean shift towards more occurrences of the negative phase PDO for the time period 2000-2099 for the B1, A1B and A2 emissions scenarios (Table 4). In particular, the A2 scenario all-model mean PDO index was projected to become significantly more negative, which is reflected in the significantly increased discharges for the Flathead, naturalized St. Mary and naturalized Belly records, whose GLS models do not include a declining trend term (Figure 3 and Table 5). More occurrences of the negative phase of the PDO are also consistent with increasing winter precipitation (Barrow, 2010). Hence, it might be expected that the PDO would only contribute to increased flow (but see paragraph below). Yet note that in the projected competing effects between the PDO terms' largely contributing to central Rocky mountain discharge, and the declining trend terms contributing to decreased flows, this study suggests that the declining trend terms dominate in the majority of the modeled river records.

In Lapp et al. (2012) not all the models showed a consistent shift to negative PDO conditions. The GCMs separate between those showing a shift, often significant, towards more negative PDO-like conditions for all three scenarios (i.e., MIROC (medres), MRI and HadCM3), and those showing a contrary shift, also often significant, towards more positive PDO-like conditions for all runs and all three scenarios (i.e., CGCM3.1 (T47) , CGCM3.1 (T63), GDFL2.1, MIROC (hires) and NCAR-PCM). If these latter GCMs are correct and the PDO

shifts into a more positive state in the 21st century, then the PDO terms in the GLS models will contribute to discharge deficits, rather than increases. PDO projections from the ongoing AR5 (CMIP5) climate prediction experiments would be valuable for projecting the regional hydroclimatology, especially if they show more consistency in the direction of PDO shift. Overland and Wang (2007) and Wang et al. (2010) examined the closely related question of when the anthropogenic global warming trend will surpass the natural variability of the North Pacific region under the A1B emissions scenario. They suggested that this will occur circa 2040-2050, leading to a weaker meridional temperature gradient in the North Pacific Region, and thereby perhaps to a weakening of its effect on the sub-polar jetstream. (The mechanism by which the PDO affects the hydroclimatology of the downstream western North America is through a shift in the position of the sub-polar jet, which brings winter storms and precipitation as it crosses over the edge of the continent (Gershunov and Barnett, 1998; Bonsal et al., 2001; Stahl et al., 2006)). Because of this result, our streamflow projections past 2050 are likely less reliable.

The reliability of our results also depends on the representativeness of the low B1, moderate A1B and severe A2 SRES emission scenarios. Recent research (van Vuuren and Riahi, 2008) compared actual measured emissions to the IPCC Special Report on Emissions Scenarios (SRES) forecast rates and showed that thus far, for 1990-2006, a high emissions scenario has been most appropriate. The growth rate of global emissions after 2000 has been about 3%, whereas the forecast growth rates under SRES had ranged from between 1.4% and 3.4%. Hence, the actual emissions have been well represented by the scenario variability so far.

These GLS model extrapolations are thought-experiments of what could happen if present-day trends in temperature, precipitation, evapotranspiration, water demand and use continue on the same path; together with the current relationships between central Rocky Mountain hydroclimatology and the atmosphere-ocean climate oscillations (as assessed over the entire centennial-length instrumental record). These projections out to 2050 do not seem unreasonable, given the shortness of the intervening time interval. They present a sobering picture of probable declines in surface water supplies in a region where water is already highly in demand and tightly allocated. Post-2050, these projections are certainly more speculative, given our assumption of no changes in the physical hydrology, such as those induced by a shift of precipitation from snow to rain and in the post-2050 North Pacific Ocean variability shifts (Overland and Wang, 2007; Wang et al., 2010), and the tendency of GCM-based post-2050 PDO projections to divide into those demonstrating strong negative PDO phase shifts and those demonstrating strong positive PDO phase shifts (Lapp et al., 2012). Nevertheless, these entire 21st century projections are a worthwhile exploration of the range of possible scenarios, highlighting probable future surface water deficits and the importance of the future behavior of the PDO upon central Rocky Mountain river discharges.

Acknowledgments

We acknowledge the international modeling groups for providing their data for analysis, the Program for Climate Model Diagnosis and Intercomparison (PCMDI) for collecting and archiving the model data, the WCRP/CLIVAR Working Group on Coupled Models (WGCM),

ACCEPTED MANUSCRIPT

and their Coupled Model Intercomparison Project (CMIP) and Climate Simulation Panels for organizing the model data analysis activity, and the IPCC WG1 TSU for technical support. This research was funded by the Natural Sciences and Engineering Research Council of Canada, Alberta Environment and Natural Resources Canada under the Regional Adaptation Collaboratives Program. We would like to thank Stewart Rood and Scott Starratt for their helpful comments which greatly improved this manuscript.

References

Alberta Environmental Protection, 1998. South Saskatchewan River basin historical weekly natural flows 1912 to 1995: Main Report and MicrosoftAccess Database. Natural Resources Services, Water Management Division, Water Sciences Branch, Edmonton.

Axelson J., Sauchyn D.J., Barichivich J., 2010. New reconstructions of streamflow variability in the South Saskatchewan River basin from a network of tree-ring chronologies, Alberta, Canada. Water Resources Research 45, W09422.

Barrow, E., 2010. Climate change scenarios for the Prairie Provinces. In: Sauchyn, D.J., H. Diaz, H., Kulshreshtha, S. (Eds.), The New Normal: the Canadian Prairies in a Changing Climate, Canadian Plains Research Center Press, Regina, Saskatchewan, pp. 41-58.

Bonsal, B., Lawford, R.G., 1999. Teleconnections between El Niño and La Niña events and summer extended dry spells on the Canadian prairies. International Journal of Climatology, 19, 1445-1458.

Bonsal, B., Shabbar, A., 2008. Impacts of large-scale circulation variability on low streamflows over Canada: a review. Canadian Water Resources Journal, 33, 137-154.

Bonsal, B., Shabbar, A., Higuchi, K., 2001. Impacts of low frequency variability modes on Canadian winter temperature. International Journal of Climatology, 21, 95-108.

Brockwell, P.J., Davis, R.A., 2002. Introduction to time series and forecasting, 2nd *ed*., Springer-Verlag, New York.

Comeau, L.E.L., Pietroniro, A., Demuth, M.N., 2009. Glacier contribution to the North and South Saskatchewan Rivers. Hydrological Processes, 23, 2640-2653.

Cryer, J.D., Chan, K.-S., 2008. Time series analysis with applications in R, 2nd *ed.*, Springer-Verlag, New York.

Day, C.A., 2009. Modelling impacts of climate change on snowmelt runoff generation and streamflow across western US mountain basins: a review of techniques and applications for water resource management. Progress in Physical Geography 33, 614-633.

Dettinger, M.D., 2005. From climate-change spaghetti to climate-change distributions for 21st century California. San Francisco Estuary and Watershed Science, 3(1) Article 4 (http://repositories.cdlib.org/jmie/sfews/vol3/iss1/art4).

ACCEPTED MANUSCRIPT

Dettinger, M.D., 2006. A component-resampling approach for estimating probability distributions from small forecast ensembles. Climatic Change 76, 149-168.

Dettinger, M.D., Cayan, D.R., Meyer, M.K., Jeton, A.E., 2004. Simulated hydrologic responses to climate variations and change in the Merced, Carson and American River basins, Sierra Nevada, California, 1900-2099. Climatic Change 62, 283-317.

Furtado, J.C., Di Lorenzo, E., Schneider N., Bond, N.A., 2011. North Pacific decadal variability and climate change in the IPCC AR4 models. Journal of Climate 24, 3049-3067.

Gershunov, A., Barnett, T.P., 1998. Interdecadal modulation of ENSO teleconnections. Bulletin of the American Meteorological Society 79, 2715-2725.

Harvey, K.D., Pilon, P.J., Yuzyk T.R., 1999. Canada's reference hydrometric basin network (RHBN). In: Partnerships in Water Resources Management. Paper presented at Canadian Water Resources Association (CWRA)'s 51st Annual Conference, June 1999, Halifax, Nova Scotia.

IPCC4, 2007. Climate Change 2007: The Physical Science Basis. Contribution of Working Group I to the Fourth Assessment Report of the Intergovernmental Panel on Climate Change (Solomon, S., Qin, D., Manning, M., Chen, Z., Marquis, M., Avery, K.B., Tignor, M., Miller, H.L. (Eds.)), Cambridge University Press, Cambridge, UK.

Jones, P.D., Jonsson, T., Wheeler, D., 1997. Extension to the North Atlantic Oscillation using early instrumental pressure observations from Gibraltar and South-west Iceland. International Journal of Climatology, 17, 1433-1450.

Kienzle, S.W., Nemeth, M.W., Bryne, J.M., McDonald, R.J., 2012. Simulating the hydrological impacts of climate change in the upper North Saskatchewan River basin, Alberta, Canada. Journal of Hydrology, 412, 76-89, DOI: 10.1016/j.jhydrol.2011.01.058.

Lapp, S., Sauchyn, D.J., Toth, B., 2009. Constructing scenarios of future climate and water supply for the SSRB: Use and limitations for vulnerability assessment. Prairie Forum 34, 153-180.

Lapp, S., St. Jacques, J.M., Barrow, E.M., Sauchyn, D.J., (2012). GCM projections for the Pacific Decadal Oscillation under greenhouse forcing for the early 21st century. International Journal of Climatology. *Early on-line* DOI: 10.1002/joc.2364.

Larson, R.P., Byrne, J.M., Johnson, D.L., Kienzle, S.W., Letts, M.G., 2011. Modelling climate change impacts on spring runoff for the Rocky Mountains of Montana and Alberta II: runoff change projections using future scenarios. Canadian Water Resources Journal 36, 35-52.

Lima, C.H.R., Lall, U., 2010. Climate informed monthly streamflow forecasts for the Brazilian hydropower network using a periodic ridge regression model. Journal of Hydrology 380, 438-449.

ACCEPTED MANUSCRIPT

MacDonald, R.J., Byrne, J.M., Kienzle, S.W., Larson, R.P., 2011. Assessing the potential impacts of climate change on mountain snowpack in the St. Mary River watershed, Montana, Journal of Hydrometeorology 12, 262-273.

Mantua, N.J., Hare, S.R., 2002. The Pacific Decadal Oscillation, Journal of Oceanography 58, 35-44.

Mantua, N.J., Hare, S.R., Zhang, Y., Wallace, J.M., Francis, R.C., 1997. A Pacific interdecadal climate oscillation with impacts on salmon production. Bulletin of the American Meteorological Society 78, 1069-1079.

Meehl, G.A., Covey, C., Delworth, T., Latif, M., McAvaney, B., Mitchell, J.F.B., Stouffer, R.J., Taylor, K.E., 2007. The WCRP CMIP3 multimodel dataset, a new era in climate change research. Bulletin of the American Meteorological Society 88, 1383-1394.

Minobe, S., 1997. A 50-70 year climatic oscillation over the North Pacific and North America, Geophysical Research Letters 24, 683-686.

Nakicenovic N., Alcamo, J., Davis, G., de Vries, B., Fenhann, J., Gaffin, S., Gregory, K., Grübler, A., Jung, T.Y., Kram, T., La Rovere, E.L., Michaelis, L., Mori, S., Morita, T., Pepper, W., Pitcher, H., Price, L., Riahi, K., Roehrl, A., Rogner, H.H., Sankovski, A., Schlesinger, M., Shukla, P., Smith, S., Swart, R., van Rooijen, S., Victor, N., Dadi, Z., 2000. IPCC Special Report on Emissions Scenarios, Cambridge University Press, Cambridge, United Kingdom and New York, NY, USA.

Overland, J.E., Wang, M., 2007. Future climate of the North Pacific Ocean. Eos 88, 178, 182.

R Development Core Team, 2008. R: A language and environment for statistical computing. R Foundation for Statistical Computing, Vienna, Austria. ISBN 3-900051-07-0, (version 2.91. used) URL http://www.R-project.org.

Rayner, N.A., Parker, D.E., Horton, E.B., Folland, C.K., Alexander, L.V., Rowell, D.P., Kent, E.C., Kaplan, A., 2003. Globally complete analyses of sea surface temperature, sea ice and night marine air temperature, 1871-2000. Journal of Geophysical Research 108, 4407, DOI 10.1029/2002JD002670.

Rood, S.B., Vandersteen, J.W., 2010. Relaxing the principle of prior appropriation: stored water and sharing the shortage in Alberta, Canada. Water Resources Management 24, 1605-1620.

Rood, S.B., Samuelson, G.M., Weber, J.K., Wywrot, K.A., 2005. Twentieth-century decline in streamflows from the hydrographic apex of North America. Journal of Hydrology 306, 215-233.

Rood, S.B., Pan, J., Gill, K.M., Franks, C.G., Samuelson, G.M., Shepherd, A., 2008. Declining summer flows of Rocky Mountain rivers: changing seasonal hydrology and probable impacts on floodplain forests. Journal of Hydrology 349, 397-410.

Ropelewski, C.F., Jones, P.D., 1987. An extension of the Tahiti-Darwin Southern Oscillation Index. Monthly Weather Review 115, 2161-2165.

ACCEPTED MANUSCRIPT

Ruiz, J.E., Cordery, I., Sharma, A., 2007. Forecasting streamflows in Australia using the tropical Indo-Pacific thermocline as predictor. Journal of Hydrology 341, 156-164.

St. Jacques, J.M., Sauchyn, D.J., Zhao, Y., 2010. Northern Rocky Mountain streamflow records: global warming trends, human impacts or natural variability? Geophysical Research Letters 37, 2009GL042045.

Sauchyn, D., Vanstone, J., Perez-Valdivia, C., 2011. Modes and forcing of hydroclimatic variability in the Upper North Saskatchewan River basin since 1063. Canadian Water Resources Journal 36, 205-218.

Schindler, D.W., Donahue, W.F., 2006. An impending water crisis in Canada's western prairie provinces. Proceedings of the National Academy of Sciences 103, 7210-7216.

Shabbar, A., Khandekar, M., 1996. The impact of El Niño-Southern Oscillation on the temperature field over Canada. Atmosphere-Ocean 34, 401-416.

Shabbar, A., Skinner, W., 2004. Summer drought patterns in Canada and the relationship to global sea surface temperatures. Journal of Climate 17, 2866-2880.

Shabbar, A., Bonsal, B., Khandekar, M., 1997. Canadian precipitation patterns associated with the Southern Oscillation. Journal of Climate 10, 3016-3027.

Shepherd, A., Gill, K.M., Rood, S.B., 2010. Climate change and future flows of Rocky Mountain rivers: converging forecast from empirical trend projection and down-scaled global circulation modeling. Hydrological Processes 24, 3864-3877.

Slack, J.R., Landwehr, J.M., 1992. Hydro-climatic data network: a U.S. Geological Survey streamflow data set for the United States for the study of climate variations, 1874-1988, United States Geological Survey Open-File Report 92-129.

Stahl, K., Moore, R.D., McKendry, I.G., 2006. The role of synoptic-scale circulation in the linkage between large-scale ocean-atmosphere indices and winter surface climate in British Columbia, Canada. International Journal of Climatology 26, 541-560.

Stewart, I., Cayan, D.R., Dettinger, M.D., 2004. Changes in snowmelt runoff timing in western North America under a "business as usual" climate change scenario. Climatic Change 62, 217-232.

Stewart, I., Cayan, D.R., Dettinger, M.D., 2005. Changes toward earlier streamflow timing across western North America. Journal of Climate 18, 1136-1155.

Tanzeeba, S., Gan, T.Y., 2012. Potential impact of climate change on the water availability of South Saskatchewan River Basin. Climatic Change 112, 355-386.

van Vuuren, D.P., Riahi, K., 2008. Do recent emission trends imply higher emissions forever? Climatic Change 91, 237-248.

ACCEPTED MANUSCRIPT

Vicuna, S., Dracup, J.A., 2007. The evolution of climate change impact studies on hydrology and water resources in California. Climatic Change 82, 327-350.

Wallace, J.M., Gutzler, D.S., 1981. Teleconnections in the geopotential height field during the Northern Hemisphere winter. Monthly Weather Review 109, 784-812.

Wang, M., Overland, J.E., Bond, N.A., 2010. Climate projections for selected large marine ecosystems. Journal of Marine Systems 79, 258-266.

Wilks, D.S., 2006. Statistical Methods in the Atmospheric Sciences, *2nd ed.*, Academic Press, New York.

Wise, E.K., 2010. Spatiotemporal variability of the precipitation dipole transition zone in the western United States. Geophysical Research Letters 37, L07706.

Xu, K., Brown, C., Kwon, H.-H., Lall, U., Zhang, J., Hayashi, S., Chen, Z., 2007. Climate teleconnections to Yangtze river seasonal streamflow at the Three Gorges Dam, China. International Journal of Climatology 27, 771-780.

Zhang, X., Vincent, L.A., Hogg, W.D., Niitsoo, A., 2000. Temperature and precipitation trends in Canada during the 20th century. Atmosphere-Ocean 38, 395-429.

Zhang, X., Harvey, K.D., Hogg, W.D., Yuzyk, T.R., 2001. Trends in Canadian streamflow. Water Resources Research 37, 987-998.

Zhang, Y., Wallace, J.M., Battisti, D.S., 1997. ENSO-like interdecadal variability: 1900-1993. Journal of Climate 10, 1004-1020.

Zheng, X., Basher, R.E., Thompson, C.S., 1997. Trend detection in regional-mean temperature series: maximum, minimum, mean, diurnal range, and SST. Journal of Climate 10, 317-326.

Table 1. Details of the 11 central Rocky Mountain discharge records, ordered by drainage and then increasing latitude. Significant linear trend as assessed following the methodology of St. Jacques et al. (2010). Low-pass variance is the variance in low-frequency filtered streamflow data as a percentage of the total variability. Mean Q_t is mean daily discharge averaged over the year. The naturalized records are from the same location as the corresponding actual flow gauge.

Flow record (HYDAT or USGS code)	Record period	Flow regime	Significant linear trend?	Low-pass variance	Gross drainage (km^2)	Mean Q_t (m^3/s)
Pacific Ocean drainage						
***North Fork Flathead R., MT* (12355500)**	1936-2008	natural	none	43.1%	4009	83.9
Elk R. at Phillips Bridge, BC* (08NK005)	1933-2008	minimally regulated	**decreasing**	40.7%	4450	75.9
Gulf of Mexico drainage						
***Marias R. near Shelby, MT* (06099500)**	1912-2007	slightly regulated	**decreasing**	45.3%	3242	25.0
Hudson Bay drainage						
***St. Mary R. at International Boundary, AB* (05AE027)**	1903-2007	regulated	**decreasing**	51.6%	1206	20.2
St. Mary R. at International Boundary	1912-2001	naturalized	none	38.9%	1206	25.1
***Belly R. near Mountain View, AB* (05AD005)**	1912-2007	slightly regulated	**decreasing**	38.5%	319	8.6
Belly R. near Mountain View	1912-2001	naturalized	none	38.6%	319	9.1
***Waterton R. near Waterton Park, AB* (05AD003)**	1912-2007	natural	**decreasing**	40.6%	613	17.6
***Oldman R. near Lethbridge, AB* (05AD007)**	1912-2007	extensively regulated	**decreasing**	52.2%	17,046	84.6
Oldman R. near Lethbridge	1912-2001	naturalized	**decreasing**	44.1%	17,046	109.6
***S. Saskatchewan at Medicine Hat* (05AJ001)**	1912-2007	extensively regulated	**decreasing**	55.0%	41,000	187.4

*1996-2008 extrapolated from Fernie (r^2 = 0.97)

ACCEPTED MANUSCRIPT

Table 2. Identification of the optimum Generalized Least Squares (GLS) equations and residual models for the 11 central Rocky Mountain streamflow records. AIC_c: corrected Akaike Information Criterion. Predictor variables are standardized to zero mean and unit standard deviation; discharge Q_t is centered to zero mean. 0, ±1, +2 year lags of climate indices included in analysis. P1: climate leads streamflow 1 year. P2: climate leads streamflow 2 years. N1: climate lags streamflow 1 year. RP: Neyman-Pearson statistic (results significant at the 10% level in bold).

Flow record	R^{2*} (regular)	R^{2**} (innovations)	AIC_c	GLS equation	Residual model	RP (*p*-level)
North Fork Flathead R.	0.53	0.75	464	$Q_t = 0.10 - 7.92*PDO - 2.21*NAO_{P1} - 4.18*PDO_{P2} - 3.39*SOI_{P2}$	ARMA(2,1)	1.1 (0.29)
Elk R. at Phillips Bridge	0.54	0.71	479	$Q_t = 0.05 - 1.75*trend - 6.66*PDO - 1.68*NAO_{N1} - 1.37*NAO_{P1} - 3.09*PDO_{P2} - 3.12*SOI_{P2}$	ARMA(2,1)	**18.2 ($2.0xe^{-5}$)**
Marias R.	0.56	0.74	526	$Q_t = 0.21 - 3.0*trend - 2.07*PDO - 1.06*NAO_{P1} - 1.21*PDO_{P1} - 2.06*PDO_{P2} - 2.44*SOI_{P2}$	ARMA(2,3)	**30.0 ($4.3xe^{-8}$)**
Actual St. Mary R.	0.61	0.75	493	$Q_t = -0.03 - 3.10*trend - 1.52*PDO + 0.80*NAO_{P2} - 1.31*PDO_{P2} - 1.50*SOI_{P2}$	ARMA(0,3)	**22.6 ($2.0xe^{-6}$)**
Naturalized St. Mary R.	0.51	0.71	394	$Q_t = -0.03 - 1.55*PDO + 0.76*SOI - 0.90*NAO_{N1} + 1.09*NAO_{P2} - 0.98*PDO_{P2} - 1.04*SOI_{P2}$	ARMA(3,2)	0.58 (0.45)
Actual Belly R.	0.55	0.64	239	$Q_t = 0.01 - 0.32*trend - 0.40*PDO + 0.34*SOI_{N1} + 0.31*NAO_{P2} - 0.47*PDO_{P2} - 0.35*SOI_{P2}$	ARMA(1,2)	**15.3 ($9.0xe^{-5}$)**
Naturalized Belly R.	0.57	0.67	214	$Q_t = 0.002 - 0.37*PDO + 0.24*SOI + 0.31*SOI_{N1} + 0.24*NAO_{P2} - 0.50*PDO_{P2} - 0.34*SOI_{P2}$	ARMA(2,1)	0.02 (0.89)
Waterton R.	0.57	0.66	359	$Q_t = 0.06 - 0.58*trend - 1.06*PDO + 0.57*SOI_{N1} - 1.06*PDO_{P2} - 0.69*SOI_{P2}$	ARMA(1,2)	**12.8 (0.0003)**
Actual Oldman R.	0.62	0.73	787	$Q_t = 0.11 - 17.17*trend - 9.25*PDO - 9.52*PDO_{P2} - 9.75*SOI_{P2}$	ARMA(2,3)	**19.7 ($9.0xe^{-6}$)**
Naturalized Oldman R.	0.49	0.65	729	$Q_t = -0.24 - 5.16*trend - 8.38*PDO - 10.02*PDO_{P2} - 10.19*SOI_{P2}$	ARMA(2,3)	**3.6 (0.06)**
S. Saskatchewan R. at Medicine Hat	0.59	0.78	899	$Q_t = -0.09 - 23.20*trend - 24.41*PDO + 12.10*SOI_{N1} + 19.19*NAO_{P2} - 14.14*PDO_{P2} - 13.23*SOI_{P2}$	ARMA(3,3)	**25.4 ($4.6xe^{-7}$)**

* $R^2_{regular}$ computed as 1 – (sum-of-squares of regression residuals/total-sum-of-squares), i.e., without modeled error adjustment.
** $R^2_{innovations}$ computed with the modeled error adjustment.

Table 3. List of the ten chosen coupled atmosphere-ocean models which archived the required fields, their details, and number of available 21st century runs per scenario.

#	IPCC4 Model ID	Country	Atmospheric resolution	Oceanic resolution	Number 21st century runs		
					B1	A1B	A2
1	**CGCM3.1(T47)**	Canada	3.7^{o}x3.7^{o} L31	1.84^{o}x1.85^{o} L29	3	3	3
2	**CGCM3.1(T63)**	Canada	2.8^{o}x2.8^{o} L31	1.4^{o}x0.9^{o} L29	1	1	0
3	**ECHAM5/MPI-OM**	Germany	1.875^{o}x1.865^{o} L31	1.5^{o}x1.5^{o} L40	2	2	1
4	**GDFL-CM2.1**	USA	2.5^{o}x2.0^{o} L24	1.0^{o}x1.0^{o} L50	1	1	1
5	**MIROC3.2(hires)**	Japan	1.125^{o}x1.12^{o} L56	0.28^{o}x0.188^{o} L47	1	1	0
6	**MIROC3.2(medres)**	Japan	2.8^{o}x2.8^{o} L20	(0.5-1.4^{o}) x1.4^{o} L43	1	1	1
7	**MRI-CGCM2.3.2**	Japan	2.8^{o}x2.8^{o} L31	(0.5-2.5^{o}) x2.0^{o} L23	5	5	5
8	**NCAR-CCSM3**	USA	1.4^{o}x1.4^{o} L26	(0.3-1.0^{o}) x1.0^{o} L40	1	1	1
9	**NCAR-PCM**	USA	2.8^{o}x2.8^{o} L18	(0.5-0.7^{o}) x0.7^{o} L32	2	2	2
10	**UKMO-HadCM3**	UK	3.75^{o}x2.5^{o} L15	1.25^{o}x1.25^{o} L20	1	1	1

ACCEPTED MANUSCRIPT

Table 4. 20th century observed mean climate indices and multi-model mean climate indices for the 20th century simulations and for the 21st century projections under the B1, A1B and A2 emission scenarios. Red values identify a future shift to a positive PDO or negative SOI (El Niño-like) or negative NAO mean state; and blue to the opposite conditions (i.e., negative PDO or positive SOI (La Niña-like) or positive NAO), relative to the 20th century simulation mean. Bold **t** denotes significant change at the $0.05 < p \leq 0.10$ level. Bold * denotes a significant change in a multi-model mean index at the $p \leq 0.05$ level, relative to the 20th century simulation mean, as assessed by a Monte Carlo *t*-test.

	Winter PDO			**Annual SOI**			**Winter NAO**		
SRES scenario	**B1**	**A1B**	**A2**	**B1**	**A1B**	**A2**	**B1**	**A1B**	**A2**
Observed mean 1900-1999	0.168			-0.098			0.485		
All-model 1900-1999 simulation mean+	-0.109	-0.075	-0.101	0.040	0.049	0.046	-0.059	-0.050	-0.060
All-model 2000-2050 mean	-0.130	-0.095	-0.129	**-0.029***	0.017	0.025	-0.019	**0.115***	**0.101***
All-model 2000-2099 mean	**-0.161**t	**-0.162***	**-0.321***	**-0.025***	0.068	**0.099***	-0.040	**0.177***	**0.161***

+Not all GCMs had 21st century projected data for all three emission scenarios, therefore their simulation runs were dropped from the multi-model simulation mean where applicable.

ACCEPTED MANUSCRIPT

Table 5. Significance of trend in the all-model mean projected streamflows for 2006-2050 and 2006-2096 for the B1, A1B and A2 SRES emissions scenarios. Significant declines at the 0.05 level are denoted by a bold red ▼; significant increases at the 0.05 level are denoted by bold blue ▲; and no significant trend by ↔. Projected percentage changes *per annum* (Δ/yr) is defined as $100*\beta_1/mean(Q)$.

Flow record	2006-2050						2006-2096					
	B1		A1B		A2		B1		A1B		A2	
	Trend	Δ/yr	Trend	Δ/yr	Trend	Δ/yr	Trend	Δ/yr	Trend	Δ/yr	Trend	Δ/yr
North Fork Flathead River	↔	-0.06	▼	-0.08	↔	-0.07	↔	-0.01	↔	-0.01	▲	0.07
Elk River	▼	-0.16	▼	-0.17	▼	-0.20	▼	-0.11	▼	-0.13	▼	-0.06
Marias River	▼	-0.67	▼	-0.74	▼	-0.74	▼	-0.63	▼	-0.71	▼	-0.48
Actual St. Mary River	▼	-0.85	▼	-0.79	▼	-0.82	▼	-1.00	▼	-0.98	▼	-0.79
Naturalized St. Mary River	↔	0.01	↔	-0.03	↔	-0.01	↔	0.01	↔	0.02	▲	0.08
Actual Belly R.	▼	-0.16	▼	-0.12	↔	-0.02	▼	-0.16	▼	-0.12	▼	-0.03
Nat. Belly R.	↔	-0.01	↔	0.02	↔	0.04	↔	0.003	▲	0.05	▲	0.11
Waterton River	▼	-0.19	▼	-0.16	▼	-0.17	▼	-0.14	▼	-0.11	↔	-0.03
Actual Oldman River	▼	-1.76	▼	-1.64	▼	-1.78	▼	-2.07	▼	-2.15	▼	-1.74
Naturalized Oldman River	▼	-0.25	▼	-0.24	▼	-0.29	▼	-0.22	▼	-0.22	▼	-0.12
S. Saskatchewan River	▼	-0.74	▼	-0.67	▼	-0.49	▼	-0.84	▼	-0.66	▼	-0.39

ACCEPTED MANUSCRIPT

ACCEPTED MANUSCRIPT

Figure captions

Figure 1. Map of the central Rocky Mountains showing the eight gauge locations located at the hydrographic apex of North America, after Rood et al. (2005).

Figure 2. Plots of the 11 central Rocky Mountain flow records, smoothed by five-point binomial filters (black lines), together with fitted multiple linear GLS regressions with ARMA modeled error terms (blue), fitted multiple linear GLS regressions without the error terms (green), and significant trend lines (red). Trend lines only shown where significant at the 10% level. Mean daily flows (m^3/s) averaged over the year are presented.

Figure 3. Central Rocky Mountain 20th century river simulations (1900-2005) and river projections (2006-2096) (daily mean flows (m^3/s), averaged over the year, smoothed by five-point binomial filters) under the A1B emissions scenario, together with observed records (1905-2007). The grey lines are the individual model runs, the heavy blue lines are all-model means of the GCM runs, and the heavy red lines are the observed river records.

Figure 4. Elk River (Pacific Ocean drainage), Marias River (Gulf of Mexico drainage) and South Saskatchewan River (Hudson Bay drainage) 20th century simulations (1900-2005) and 21st century projections (2006-2096) (daily mean flows (m^3/s), averaged over the year, smoothed by five-point binomial filters) under the B1, A1B and A2 emissions scenarios, together with observed records (1905-2007). The grey lines are the individual model runs, the heavy blue lines are all-model means of the GCM runs, and the heavy red lines are the observed river records.

Figure 5. Projection distributions of projected lightly smoothed annual discharges (five-year binomial smoother) for the 11 Central Rocky Mountain river records in response to 20,000 climate-change realizations based upon 51 GCM streamflow projections, following the methodology of Dettinger (2005, 2006).

Figure 6. Empirical cumulative frequency distributions of projected lightly smoothed annual discharges (five-year binomial smoother) for the Elk River (Pacific Ocean drainage), Marias River (Gulf of Mexico drainage) and South Saskatchewan River (Hudson Bay drainage) records in response to 20,000 climate-change realizations based upon 51 GCM streamflow projections, following the methodology of Dettinger (2005, 2006).

ACCEPTED MANUSCRIPT

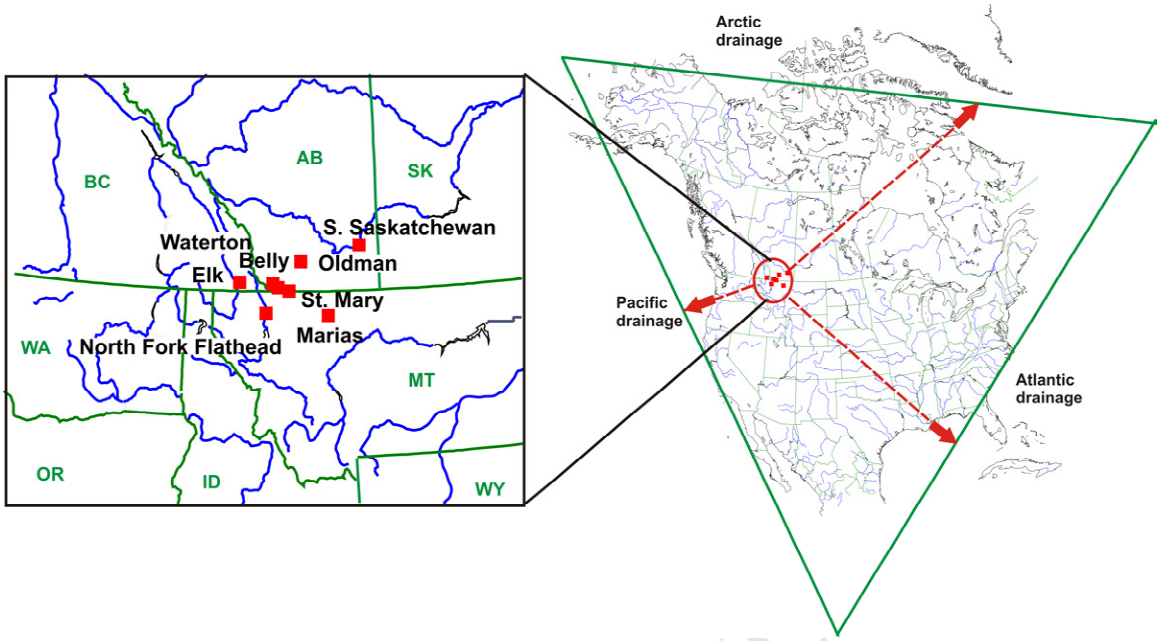

ACCEPTED MANUSCRIPT

ACCEPTED MANUSCRIPT

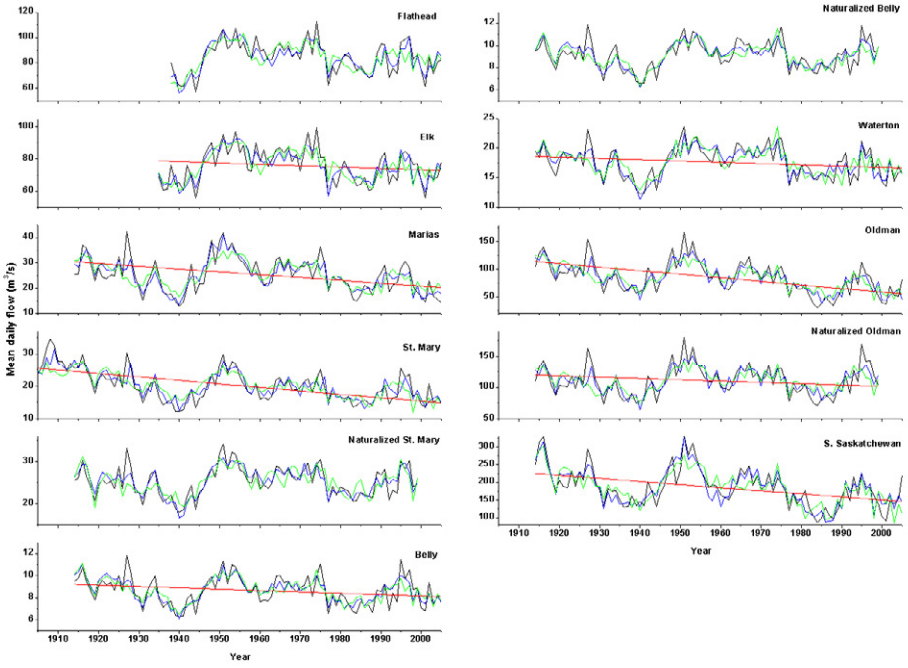

ACCEPTED MANUSCRIPT

ACCEPTED MANUSCRIPT

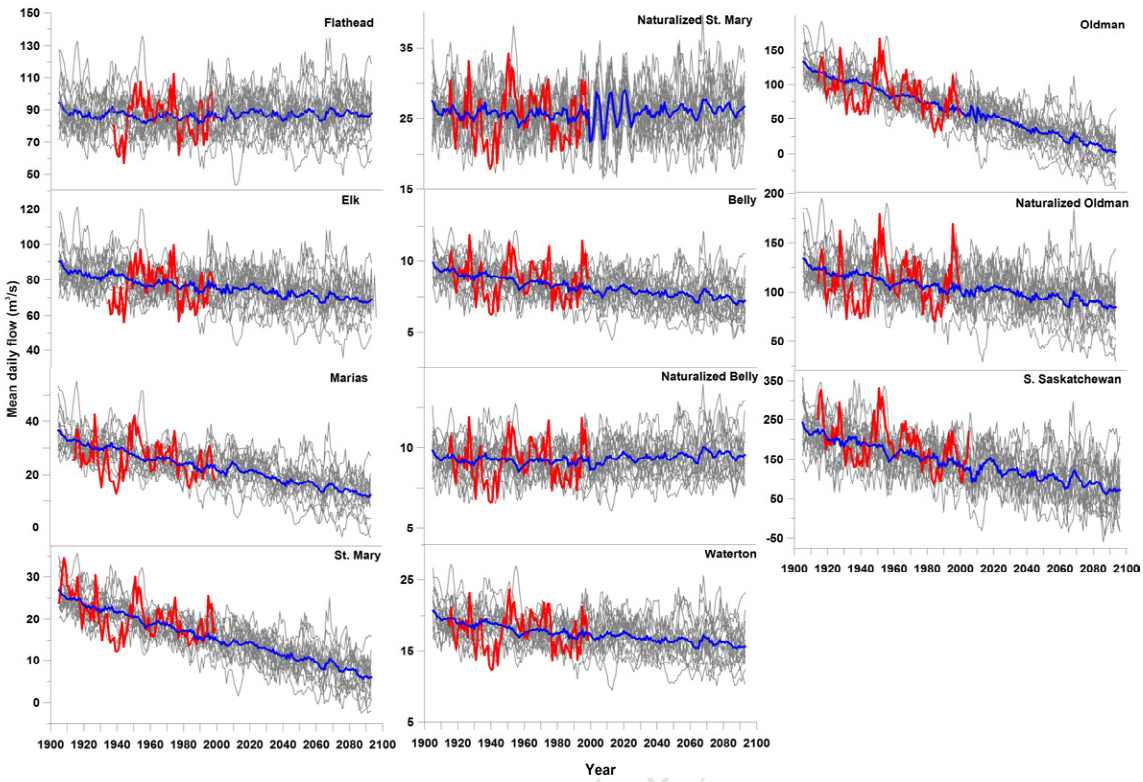

ACCEPTED MANUSCRIPT

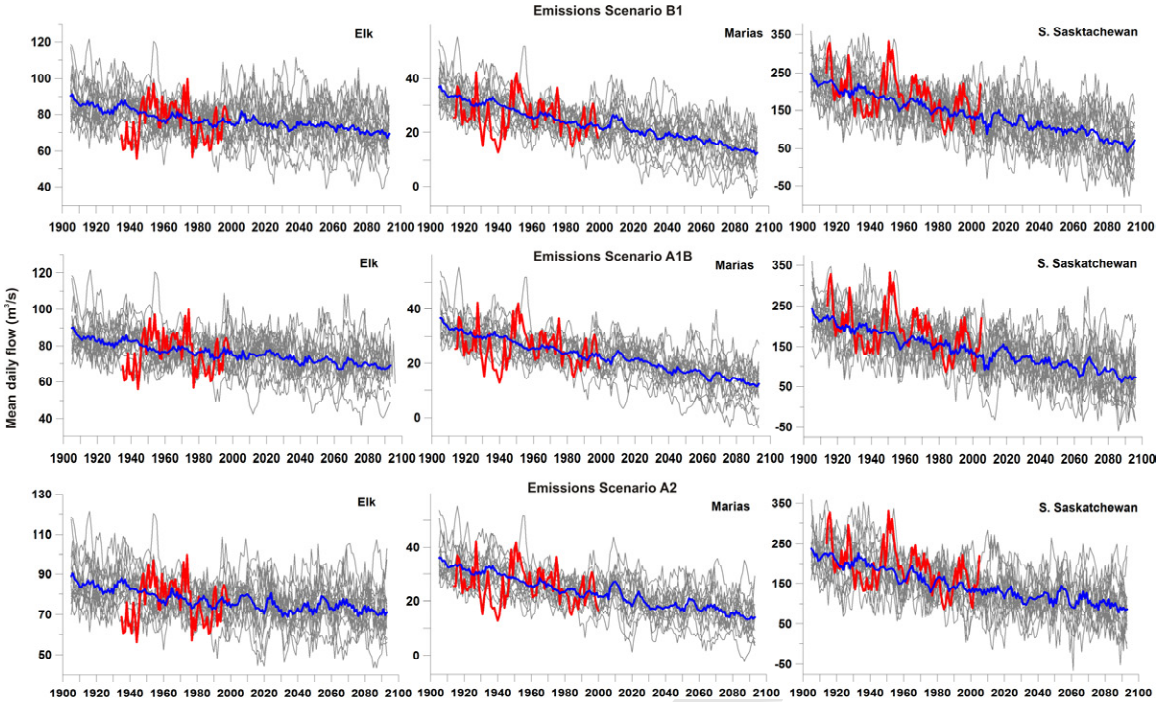

ACCEPTED MANUSCRIPT

ACCEPTED MANUSCRIPT

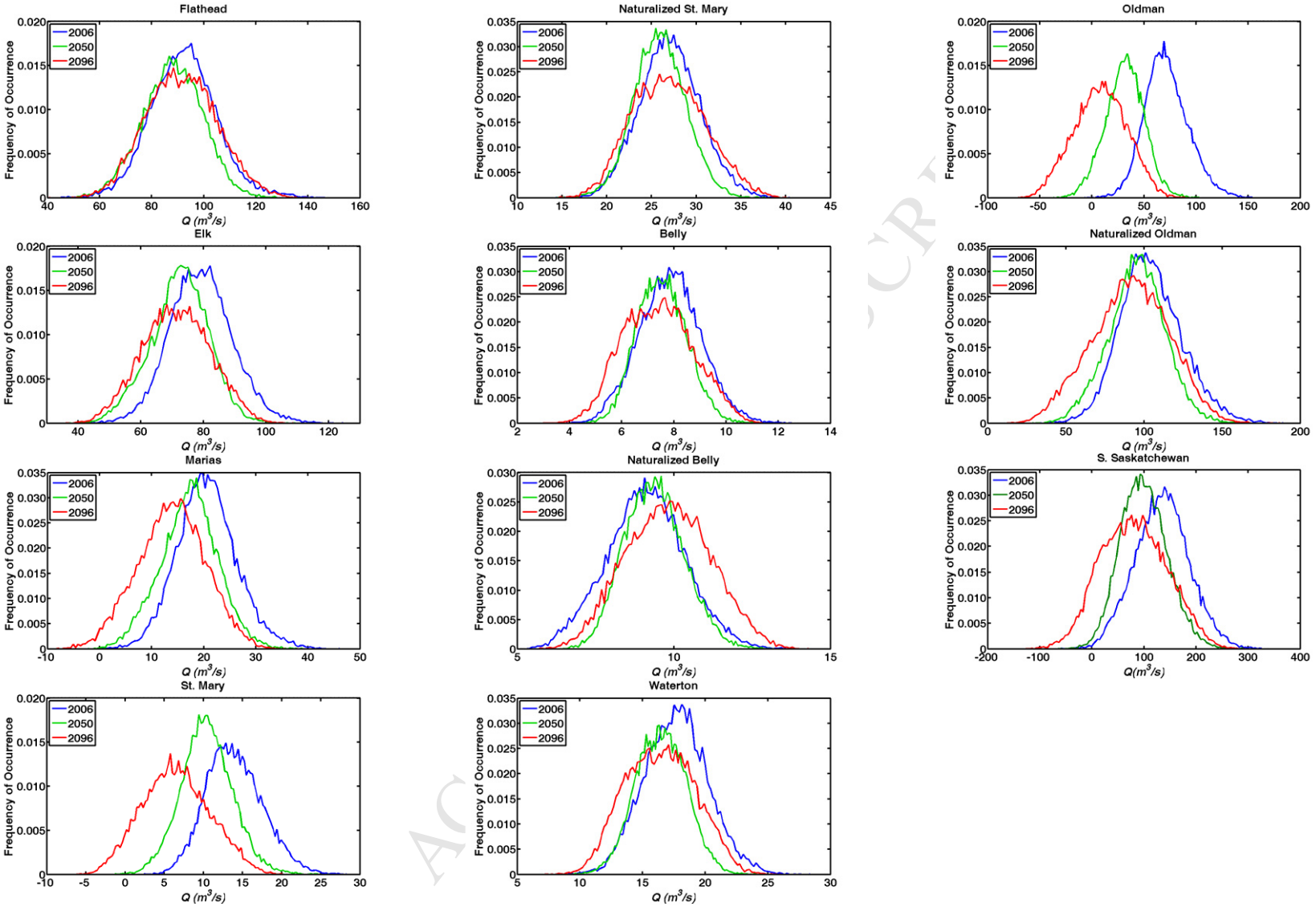

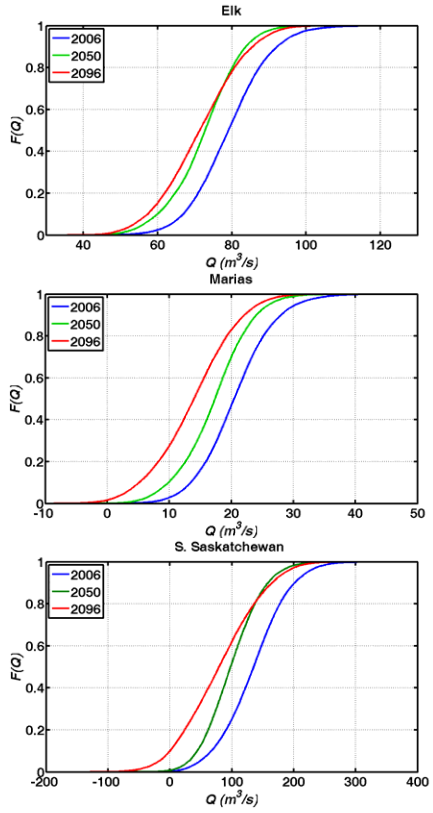

ACCEPTED MANUSCRIPT